Modelling of the bead formation during multi pass hybrid laser/gas metal arc welding

Olivier Desmaison, Gildas Guillemot, Michel Bellet

LASERAP'7, Séminaire européen sur les applications des lasers de puissance, Ile d'Oléron, 1-5 octobre 2012, Proc. published online: https://docs.google.com/file/d/0B8_nHgriy_TUQkJiZUhMVUluM0E/edit (2012) 155-161

Modelling of the bead formation during multi pass hybrid laser/gas metal arc welding

Olivier DESMAISON, Gildas GUILLEMOT, Michel BELLET

Mines ParisTech, CEMEF – Centre de Mise en Forme des Matériaux, CNRS UMR 7635, Sophia Antipolis, France
olivier.desmaison@mines-paristech.fr

Abstract

A three dimensional finite element model has been developed to simulate weld bead formation in multi pass hybrid laser/gas metal arc welding. The model considers both a gas metal arc welding (GMAW) electrode and a laser beam moving along a workpiece. A Eulerian approach is used in which the interface between the metal and the surrounding gas or plasma is defined by a level set function. Therefore heat transfer boundary conditions are applied through a "Continuum Surface Force" model. An original method has been settled to model material supply. A volume expansion source term is added to the right hand side of the mass conservation equation for certain liquid finite elements in the fusion zone. A compressible Navier Stokes equation is then solved. The new obtained velocity field is used to solve the transport of the level set function for the updating of the gas/metal interface. A new topological reinitialization method has been developed to hold the Eikonal property in the compressible framework of the level set transport. The efficiency of this global model enables to simulate industrial multi pass hybrid welding processes.

1. Introduction

The large use of welding processes in heavy industries has lead scientists to take an interest in the welding modelling. The understanding of weld pool dynamics and solidification during gas metal arc welding (GMAW) is of great importance to master the shape of fusion and heat affected zones, the shape of weld beads, and the formation of deformations and stresses in the neighbourhood of the fusion zone. Moreover, these stresses may lead to hot tearing for some critical alloys and highlights the need for accurate numerical modelling. Recently the efficiency of GMAW processes has been enhanced through the coupling with a laser beam. Located ahead of the torch, this new heat source provides additional energy to the workpiece. The resulting weld pool spreading enables to supply more material, to mix it more homogeneously and consequently to weld better and faster.

Since the development of 2D-axi stationary models for gas tungsten arc welding (GTAW) processes at the beginning of the 90's [1, 2, 3, 4] significant progress have been made. Recent models are now able to realistically simulate GMAW processes taking into account the main phenomena inside both the arc plasma and the weld pool [5, 6, 7]. The heat and mass transfer models are continuously improved. The simplified Goldak approach and the laminar flows analysis in the weld pool tend to be replaced by more physical coupled models including a Gaussian heat flux and turbulent flows without any arbitrary enhanced viscosity [8, 9, 10, 11]. Regarding free surface deformation, surface tension and arc pressure are also taken into account in the minimization of the surface energy [12, 13, 14]. Because of the progress in hybrid welding modelling and the research focus on keyhole phenomenon these numerical methods have been carried over laser/GMAW modelling [15, 16, 17, 18, 19]. As a result, the numerically obtained bead shapes better fit the experimental ones [20]. Nevertheless, only a very few models consider the entirety of the previous phenomena. Kumar and DebRoy [12], for instance, propose an advanced GMAW model in 3D, but limited to stationary and laminar conditions. Recently Wang *et al.* [21] have developed a 3D transient model for laser keyhole welding through the volume of fluid (VOF) approach to study the temperature field evolution. Results are promising but no material supply is taken into account.

The present paper reports on a transient three dimensional finite element model that has been developed to simulate the weld bead forming during multi pass hybrid laser/GMAW. The model considers both a consumable electrode and a laser beam moving along a workpiece (Figure 1-a). However the electrode, the arc plasma, the

droplets and the laser beam are not explicitly represented. The model includes the workpiece and a surrounding gaseous domain with which different boundary conditions are expressed. The plasma over the fusion zone, and the mix of air and protection gas surrounding the formed joint are parts of this domain. In the present study, the laser is supposed defocused and therefore does not give birth to the keyhole phenomenon.

The paper will present first the mathematical formulation of the finite element problem. The three main governing conservation equations – mass, energy and momentum equations – will be detailed. Secondly a multi pass hybrid laser/GMAW operation will be described. Lastly, the numerical results will be analyzed and the performance and efficiency of the model will be discussed.

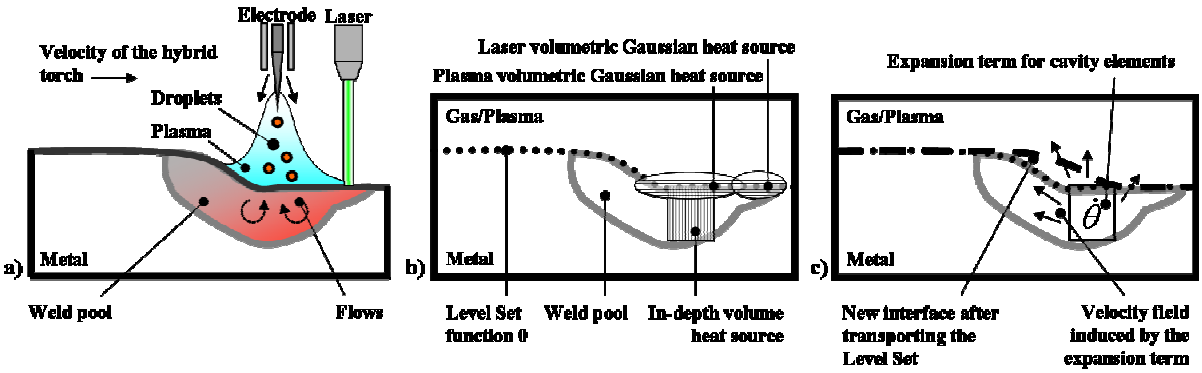

Figure 1. *Hybrid laser - GMAW model description according to the governing equations: schematic industrial process (a), energy equation model (b), material supply model (c).*

2. Mathematical formulation

2.1. Level Set approach

A Eulerian approach is used in which the interface between the metal and the surrounding air or plasma is defined by a level set function (Figure 1-b/c). Contrary to a Lagrangian approach, the chosen one enables to overcome the numerical difficulties induced by the onset of material/material contacts in multi pass welding. A nodal signed distance function φ is defined to represent the interface between gas and metal. To ensure the finite element resolution of the governing equations the material properties are averaged near the interface, using a mixed law defined as a sinusoidal Heaviside function H(φ).

$$H(\varphi)=1/2\left[1+\varphi/\varepsilon+1/\pi\left(\sin\pi\varphi/\varepsilon\right)\right] \text{ for } \varphi\in\left[-\varepsilon,+\varepsilon\right] \quad (1)$$

The mixed law is restricted to a [-ε, +ε] domain perpendicular to the surface defined by $\varphi=0$. Being α_{gas} and α_{metal} the values of a physical variable in both domains, the averaged or mixed value α is equal, in the whole model, to:

$$\alpha=\alpha_{metal}[1-H(\varphi)]+H(\varphi)\alpha_{gas} \quad (2)$$

All model's physical parameters such as ρ, C_p, λ, η are computed according to this equation, using the same Heaviside function.

2.2. Heat transfer and energy equation

The non steady-state energy equation is:

$$\rho C_p\left(\frac{\partial T}{\partial t}+\vec{v}\cdot\vec{\nabla}T\right)-\vec{\nabla}\cdot\left(\lambda\vec{\nabla}T\right)=\dot{Q} \quad (3)$$

ρ, C_p and λ are respectively the density, the equivalent specific heat and the thermal conductivity. The energy equation is solved for the temperature field. Therefore, in order to take into account the latent heat associated with fusion and solidification, the equivalent specific heat is computed following Morgan's model:

$$C_p = \left(H^t - H^{t-\Delta t}\right) / \left(T^t - T^{t-\Delta t}\right) \quad (4)$$

where the enthalpy curve *H(T)* is an input of the model. In the present model, the flows in the weld pool are not taken into account and the velocity field $\vec{v}$ is supposed null. To offset the flows and natural convection lack, the material mixing is modelled by an enhanced conductivity in the weld pool. *Q* corresponds to a heat source term. The time discretization of the energy equation is fully implicit. Once the new temperature obtained, the thermo-mechanical properties are updated.

The arc plasma supplies a surface heat flux on the interface which can be modelled by a Gaussian distribution Q_P. However, the level set framework makes impossible to impose this boundary condition on the interface as a Neumann condition because the interface is not explicitly discretized. So the Continuum Surface Force method, developed by Brackbill [22], has to be used to transform the surface boundary condition into a volumetric source term, as in [15, 16]. This method is based on the following equality:

$$\int_S \dot{Q}_P d\Gamma = \int_V \dot{Q}_P \delta(\varphi) d\Omega \quad (5)$$

with *S* and *V* respectively the surface of the interface and the volume of the model. The Dirac function $\delta(\varphi)$ is the derivative of the Heaviside function. In order to respect the equality of Eq. (5) Dirac function's integral in the [–ε, +ε] domain and in the normal direction of the interface has to be equal to one.

The same method is used for the heat source induced by the defocused laser beam. A second Gaussian distribution Q_L is applied on the interface and multiplied by the Dirac function. Heat convection and radiation effects are also taken into account through a third volume distribution Q_T.

Finally, an additional volumetric source term is defined to model the impingement of molten droplets of filler metal in the pool. According to the initial model of Lancaster [23], modified in [24], all the nodes included in a cylindrical cavity defined just below the torch beam get an extra heat source term Q_D as in [7, 9, 12, 14]. The value of Q_D mainly depends on the temperature of the droplets and the current intensity. Thus, the total volumetric heat source term *Q* of Eq. (3) is equal to:

$$\dot{Q} = \left(\dot{Q}_P + \dot{Q}_L - \dot{Q}_T\right)\delta(\varphi) + \dot{Q}_D \quad (6)$$

2.3. Material supply and deformation surface forces

In the mechanical problem, an original method has been settled to model material supply [25]. A volume expansion source term $\dot{\theta}$ is added to the right hand side of the mass conservation equation for elements contained in the cylindrical cavity described in §2.2. It is computed as a function of the geometrical dimensions of the electrode and the welding parameters. This approach to model the bead shaping is not sufficient to be realistic and the volumetric forces which deform the free surface have to be taken into account. In the present model, only two phenomena are considered: gravity F_g and surface tension F_γ. The arc pressure is neglected. Gravity is applied on the whole model as a volumetric force but to consider the surface tension force F_γ, once again, the Continuum Surface Force method must be used. The corresponding surface tension volumetric force, $F_{\gamma vol}$, is given as a function of the mean curvature κ and the surface tension term γ, using the Dirac function:

$$\vec{F}_{\gamma-vol} = \kappa\, \gamma\, \vec{n}\, \delta(\varphi) \quad (7)$$

An asset of the level framework is to easily compute the normal vector and the curvature, as follows:

$$\vec{n} = \vec{\nabla}\varphi / \|\nabla\varphi\| \text{ and } \kappa = -\nabla \cdot \vec{n} \quad (8)$$

2.4. Fluid problem resolution and level set transport

Once the energy equation solved and the thermo physical properties of the liquid/solid phases updated, the fluid problem resolution is carried over. In addition to both bead shaping forces which appear in the right hand side of the Navier Stokes equation, the expansion term is added to the right hand side of the mass conservation equation to model the bead forming. Thus, the full fluid problem to be solved is the following:

$$\rho\left(\frac{\partial \vec{v}}{\partial t}+\vec{v}\cdot\vec{\nabla}\vec{v}\right)-\vec{\nabla}\cdot\overline{\overline{\sigma}}=\vec{F}_{\gamma-vol}+\vec{F}_g \qquad with \qquad \overline{\overline{\sigma}}=\eta\left(\vec{\nabla}\vec{v}+\vec{\nabla}\vec{v}^{T}\right)$$
$$\vec{\nabla}\cdot\vec{v}=\dot{\theta} \tag{9}$$

In the context of the present study, and as a first approach, a Newtonian behaviour is assumed for both the gas and the metal. The compressible Navier Stokes equations are solved using P1+/P1 stabilized elements, with a coupled SUPG and a variational multiscale method [26]. Then in the level set approach, the signed distance function must be convected to take into account the interface deformation and, by this way, to model the bead shaping. The velocity field $\vec{v}$, obtained from the Navier Stokes equations resolution, is used to solve the convection equation of the level set [27]:

$$\frac{\partial \varphi}{\partial t}+\vec{v}\cdot\vec{\nabla}\varphi=0 \tag{10}$$

Thus, the new zero value level set represents the new metal/gas interface and takes into account the material supply. In total, this method is comparable to the resolution of the deformation surface energy minimization problem as presented in [12, 13, 14, 15, 16, 20].

2.5. Reinitialization of the level set

The level set transport is always coupled with a reinitialization method which holds the respect of the Eikonal property: after the level set advection, the norm of the distance function gradient has to be maintained equal to one, $||\nabla\varphi||=1$. For that, a modified convection equation is solved. Usually it is coupled to the transport equation for more efficiency and less computational time resolution [27]. Nevertheless, in the compressible approach of the material supply method described above, the common level set reinitialization does not provide acceptable results. A new topological method has been settled. Based on the works of Elias *et al*. [28], it consists in propagating the level set in the whole mesh from the zero isovalue level set. The method takes the advantage of being only geometrical and relies on the mesh topology. An enhancement concerning the sorting of the "to solve elements list" of the initial method has been proposed to allow the level set propagation through the heterogeneous mesh of welding simulations.

3. Model description

Table 1. *Material properties for 16MnNiMo (ASME AS533)*

Nomenclature	Symbol	Value	Nomenclature	Symbol	Value
Solidus and liquidus temperature	T_S T_L	1690 1740 K	Solid and liquid specific heat	C_{p-S} C_{p-L}	450 625 $J.kg^{-1}.K^{-1}$
Density	ρ_S ρ_L	7800 $kg.m^{-3}$	Solid and liquid viscosity	η_S η_L	10^6 0.5 $Pa.s$
Solid and liquid thermal conductivity	λ_S λ_L	37 $W.m^{-1}.K^{-1}$ 32.5× f_{λ_L}	Latent heat of fusion	L_f	2.5×10^5 $J.kg^{-1}$
Thermal conductivity factor [12]	f_{λ_L}	20	Surface tension	γ	60×10^{-3} $N.m^{-1}$

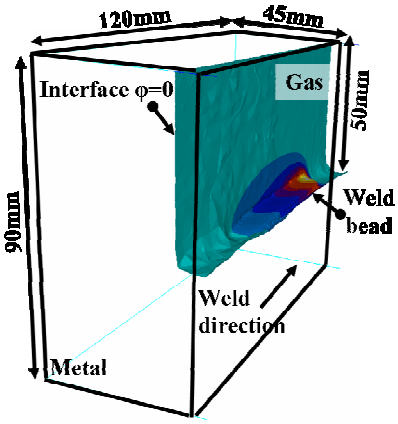

Figure 2. *Hybrid welding model.*

The finite element model consists of a parallelepiped 90 mm high, 120 mm long and 90 mm wide. A chamfer of 50 mm depth and 12 mm wide passes, lengthwise, through the workpiece, *Figure 2*. The interface between the chamfer inside and the gas is defined by the level set function. A hybrid heat source moves along the workpiece to form the weld bead. It is composed of a GMAW electrode and a 3 mm radius laser beam located 3 mm ahead. To fill one layer two passes are needed. Three passes are modelled. The power of the laser beam is 6000 W and the torch power is

10000 W, assumed to be divided in two parts: 70% for the arc plasma source and 30% for melting the electrode metal into droplets. The velocity of the torch is 13.3 mm/s, the velocity and the diameter of the wire are respectively v_w = 200 mm/s and ϕ_w = 1.2 mm. The material is a low C mid-alloyed steel 16MnNiMo or ASME SA533. Material properties, found in the literature, [29, 30, 31], are given in *Table 1*. According to literature models where the flows are not taken into account, a thermal conductivity factor f_{λ_L} is used to model the material mixing into the weld pool.

4. Results and discussion

The weld bead forming during the first pass is presented in *Figure 3*. The view is shot from a longitudinal cut plane inside the chamfer and only the metal/gas interface is visible (such as shown in *Figure 2*). For three different steps, the temperature field is displayed and the weld pool is drawn by a white line.

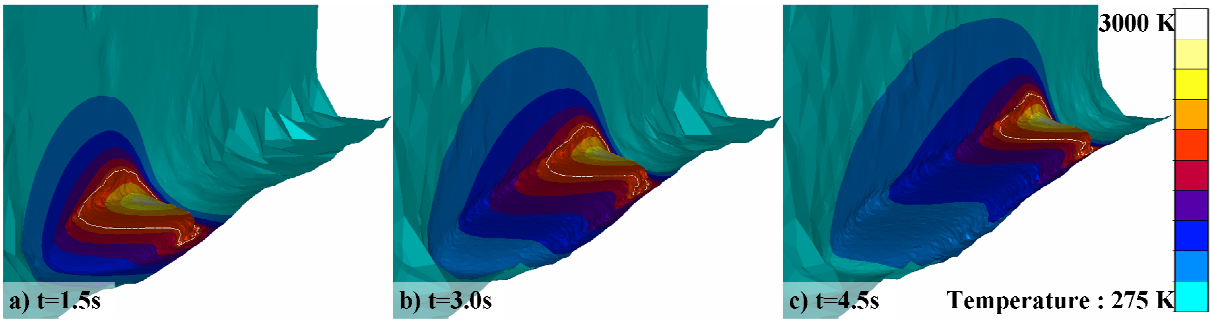

Figure 3. *Weld bead forming and temperature field at: t = 1.5 s (a), t = 3.0 s (b), t = 4.5 s (c).*

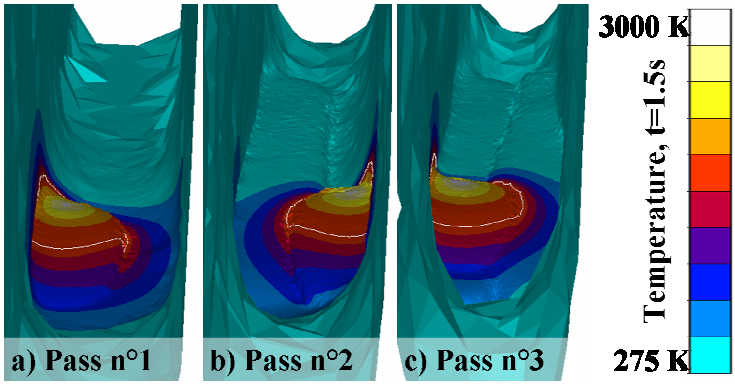

Figure 4. *Filling of the chamfer from 3 passes at the same time t = 1.5 s after each pass has started. Temperature field distribution on the metal/gas interface for the first pass (a), the second one (b) and the third one (c).*

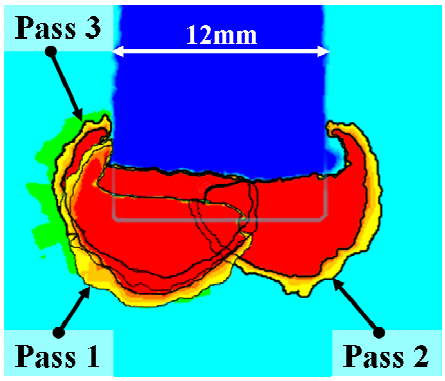

Figure 5. *Over lapping of the three weld beads in an orthogonal section plane.*

Step by step the bead is forming. The temperature field follows correctly the hybrid torch and the weld pool stays ahead the bead. The computed temperatures are in the range of experimental welding ones. Adaptive meshing tools are used to catch the interface close to the bead: refined mesh areas are computed around the bead zero isovalue level set and in the weld pool. That is why the interface which models the chamfer bottom is not smooth far from the torch. As the torch goes along, the mesh is refined ahead.

The progressive filling of the chamfer is shown in *Figure 4*. The use of the level set function allows easily managing the overlapping of the beads resulting from each pass. The three orthogonal bead profiles are superimposed in *Figure 5*. The shape of the beads qualitatively corresponds to the ones experimentally observed. The computed material supply height after two passes is around 4 mm matching the measured height. A full campaign of instrumented welding tests is planned in a near future and will permit a more quantitative evaluation of the accuracy of the model predictions.

The first pass has been simulated without the laser beam in order to analyze the assets of a hybrid welding. The comparison between the two situations is presented in *Figure 6*. The white contour lines represent the two heat sources. As expected, the additional heat flux source from the laser beam causes the spreading of the weld pool in

both longitudinal and orthogonal directions. As a consequence, the hybrid welding bead is larger but also forms more ahead of the torch in the hybrid case. This can be explained by the fact that although the cavity that is supposed to be the impingement zone for droplets is located in the same position in both cases, the supplied material spreads throughout the weld pool. It will be interesting, in a near future, to compare such prediction with weld pool surface profiles recorded through high speed cameras. It might be expected that such a comparison would reveal the need to take into account the arc pressure effect in the numerical model.

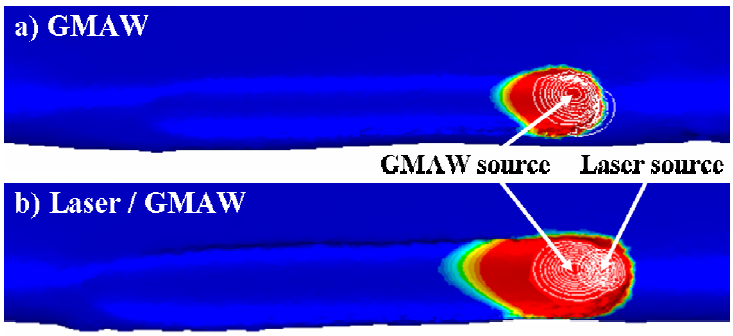

Figure 6. *Comparison of two beads obtained from (a) a GMAW simulation and (b) a hybrid Laser/GMAW simulation.*

5. Conclusion

A new transient three dimensional finite element model has been developed to simulate hybrid laser/GMAW industrial processes. The Eulerian level set approach chosen to overcome the numerical difficulties induced by bi-material contacts from multi pass welding is coupled to a new material supply modelling method. The addition of a volume expansion term in the mass conservation equation provides, after resolving Navier-Stokes equations, a velocity field which models the bead forming. The use of the *Continuum Surface Force Method* enables to transform surface boundary conditions into volumetric ones around the interface. To complete the model, a new level set reinitialization method has been implemented: the transport of the distance function is now possible in a compressible fluid area. The simulation of an industrial process from this model has highlighted realistic results regarding the weld bead shapes and the temperature field distribution. Moreover the efficiency of the model is reinforced by the adaptative meshing tools: the weld pool and the interface of the new beads are well represented through refined mesh areas. Moreover, this model turns out helpful to understand the assets of a hybrid welding.

6. Acknowledgment

This work has been supported by the French Agence Nationale de la Recherche (ANR) in the framework of the project "SISHYFE" (ANR-09-MAPR-0019).

References

[1] R.T.C. Choo, J. Szekely, and R.C. Westhoff. On the calculation of the free surface temperature of gas-tungsten-arc weld pools from first principles: Part i. modelling the welding arc. *Metallurgical Transactions B*, 23:357–369, 1992.

[2] R.T.C. Choo, J. Szekely, and S.A. David. On the calculation of the free surface temperature of gas-tungsten-arc weld pools from first principles: Part ii. modelling the weld pool and comparison with experiments. *Metallurgical Transactions B*, 23:371–384, 1992.

[3] H. G. Fan, H. L. Tsai, and S. J. Na. Heat transfer and fluid flow in a partially or fully penetrated weld pool in gas tungsten arc welding. *International Journal of Heat and Mass Transfer*, 44:417–428, 2001.

[4] L Fenggui, Y. Shun, L. Songnian, and L. Yongbing. Modelling and finite element analysis on gtaw arc and weld pool. *Computational Materials Science*, 29:371–378, 2004.

[5] J. Hu and H.L. Tsai. Heat and mass transfer in gas metal arc welding. part i: The arc. *International Journal of Heat and Mass Transfer*, 50:833–846, 2007.

[6] J. Hu and H.L. Tsai. Heat and mass transfer in gas metal arc welding. part ii: The metal. *International Journal of Heat and Mass Transfer*, 50:808–820, 2007.

[7] G. Xu, J. Hu, and H.L. Tsai. Three-dimensional modelling of arc plasma and metal transfer in gas metal arc welding. *International Journal of Heat and Mass Transfer*, 52:1709–1724, 2009.

[8] K. Hong, D.C. Weckman, A.B. Strong, and W. Zheng. Modelling turbulent thermofluid flow in stationary gas tungsten arc weld pools. *Science and Technology of Welding & Joining*, 7:125–136, 2002.

[9] J. Jaidi and P. Dutta. Three-dimensional turbulent weld pool convection in gas metal arc welding process. *Science and Technology of Welding & Joining*, 9:407–414, 2003.
[10] N. Chakraborty and S. Chakraborty. Modelling of turbulent molten pool convection in laser welding of a copper-nickel dissimilar couple. *International Journal of Heat and Mass Transfer*, 50:1805–1822, 2007.
[11] B. Ribic, R. Rai, and T. Debroy. Numerical simulation of heat transfer and fluid flow in gta/laser hybrid welding. *Science and Technology of Welding & Joining*, 13:683–693, 2008.
[12] A. Kumar and T. DebRoy. Heat transfer and fluid flow during gas-metal-arc fillet welding for various joint configurations and welding positions. *Metallurgical and Materials Transactions A*, 38:506–519, 2007.
[13] G. Xu and C. Wu. Numerical analysis of weld pool geometry in globular-transfer gas metal arc welding. *Frontiers of Materials Science in China*, 1:24–29, 2007.
[14] C.-H. Kim, W. Zhang, and T. DebRoy. Modelling of temperature field and solidified surface profile during gas-metal arc fillet welding. *Journal of Applied Physics*, 94:2667–2679, 2003.
[15] H. Ki, J. Mazumder, and P. Mohanty. Modelling of laser keyhole welding: Part i. mathematical modelling, numerical methodology, role of recoil pressure, multiple reflections, and free surface evolution. *Metallurgical and Materials Transactions A*, 33:1817–1830, 2002.
[16] H. Ki, J. Mazumder, and P. Mohanty. Modelling of laser keyhole welding: Part ii. simulation of keyhole evolution, velocity, temperature profile, and experimental verification. *Metallurgical and Materials Transactions A*, 33:1831–1842, 2002.
[17] H. Zhao and T. Debroy. Macroporosity free aluminum alloy weldments through numerical simulation of keyhole mode laser welding. *Journal of Applied Physics*, 93:10089–10097, 2003.
[18] R. Rai, S.M. Kelly, R. P. Martukanitz, and T. DebRoy. A convective heat-transfer model for partial and full penetration keyhole mode laser welding of a structural steel. *Metallurgical and Materials Transactions*, 39:98–112, 2008.
[19] T. Zhang, C.S. Wu, G.L. Qin, X.Y. Wang, and S.Y. Lin. Thermomechanical analysis for laser + gmaw-p hybrid welding process. *Computational Materials Science*, 47:848–856, 2010.
[20] A. Traidia and F. Roger. Numerical and experimental study of arc and weld pool behaviour for pulsed current gta welding. *International Journal of Heat and Mass Transfer*, 54:2163–2179, 2011.
[21] R. Wang, Y Lei, and Y Shi. Numerical simulation of transient temperature field during laser keyhole welding of 304 stainless steel sheet. *Optics & Laser Technology*, 43:870–873, 2011.
[22] J.U. Brackbill, D.B. Kothe, and C. Zemach. A continuum method for modelling surface tension. *Journal of Computational Physics*, 100:335–354, 1991.
[23] J.F. Lancaster. The physics of welding. *Physics in technology*, 15, 1984.
[24] S. Kumar and S.C. Bhaduri. Three-dimensional finite element modelling of gas metal-arc welding. *Metallurgical Transactions B*, 25:435–441, 1994.
[25] M. Bellet and M. Hamide. Direct modelling of material deposit and identification of energy transfer in gas metal arc welding. *International Journal of Numerical Methods for Heat & Fluid Flow*, Accepted, 2012.
[26] E. Hachem, T. Kloczko, H. Digonnet, and T. Coupez. Stabilized finite element solution to handle complex heat and fluid flows in industrial furnaces using the immersed volume method. *International Journal for Numerical Methods in Fluids*, 64:Online, 2010.
[27] L. Ville, L. Silva, and T. Coupez. Convected level set method for the numerical simulation of fluid buckling. *International Journal for Numerical Methods in Fluids*, 66:324–344, 2011.
[28] R.N. Elias, M.A.D. Martins, and A.L.G.A. Coutinho. Simple finite element-based computation of distance functions in unstructured grids. *International journal for numerical methods in engineering*, 72:1095–1110, 2007.
[29] M. Coret, S. Calloch, and A. Combescure. Experimental study of the phase transformation plasticity of 16mnd5 low carbon steel induced by proportional and nonproportional biaxial loading paths. *European Journal of Mechanics A/Solids*, 23:823–842, 2004.
[30] M. Coret, S. Calloch, and A. Combescure. Experimental study of the phase transformation plasticity of 16mnd5 low carbon steel under multiaxial loading. *International Journal of Plasticity*, 18:1707–1727, 2002.
[31] Y. Vincent, J.F. Jullien, and P. Gilles. Thermo-mechanical consequences of phase transformations in the heat-affected zone using a cyclic uniaxial test. *International Journal of Solids and Structures*, 42:4077–4098, 2005.